JOBS
مجلة العلوم الأساسية
Journal of Basic Science
Print -ISSN 2306-5249
Online-ISSN 2791-3279
العدد السادس والأربعون
٢٠٢٦م /١٤٤٨هـ

(350)- (325)
العدد السادس والأربعون

تأثير عدد الرشات على التبلور والعيوب التركيبية والأداء البصري لأغشية أكسيد الزنك الرقيقة المرسبة بواسطة الرش الحراري الكيميائي

م. م. احمد تركي عبد الحميد
قسم الفيزياء، كلية التربية للعلوم الصرفة، جامعة الحمدانية
Phy.ahmedturki@uohamdaniya.edu.iq
م. د. معتزبالله إبراهيم عبدالله
وزارة التربية، المديرية العامة للتربية في محافظة كركوك، متوسطة الجوهرة للبنات
mutazalalmi1990@gmail.com
م. د. شهد احمد ذياب
قسم الفيزياء، كلية التربية للعلوم الصرفة، جامعة تكريت، تكريت العراق
shahed.ahmed@tu.edu.iq

المستخلص:

تم ترسيب أغشية رقيقة من أكسيد الزنك (ZnO) على ركائز زجاجية باستخدام تقنية الرش الحراري الكيميائي، وذلك بتطبيق عدد رشات مختلفة (٢٠، ٢٥، و٣٠)، والتي سُميت على التوالي S1، S2، وS3. دُرس تأثير عدد الرشات على الخصائص البنيوية والمورفولوجية والبصرية للأغشية باستخدام حيود الأشعة السينية (XRD)، والمجهر الإلكتروني الماسح ذي الانبعاث الميداني (FE−SEM)، ومجهر القوة الذرية (AFM)، ومطيافية الأشعة فوق البنفسجية والمرئية. أكد تحليل حيود الأشعة السينية (XRD) تكون أكسيد الزنك متعدد البلورات أحادي الطور ذي بنية (Wurtzite crystal structure) سداسية. أدى زيادة عدد الرشات إلى تحسين التبلور، مما أسفر عن زيادة في حجم البلورات من ٢٧,٧ إلى ٣٤,١ نانومتر، بينما انخفضت كثافة الإجهاد الميكروي وكثافة الانخلاعات من $4.45x10^{-3}$ إلى $3.48x10^{-3}$ ومن $1.31x10^{15}$ إلى $0.86x10^{15}$ م$^{-٢}$ على التوالي. وكشفت ملاحظات المجهر الإلكتروني الماسح ذي الانبعاث الميداني (FESEM) عن نمو الحبيبات من حوالي ١٦٠ نانومتر الى ٣٥٠ نانومتر مع تحسن في كثافة الفيلم وتجانس السطح. وأظهرت نتائج مجهر القوة الذرية (AFM) زيادة في أقصى ارتفاع للسطح من ٦١,٥٧ إلى ٨٤,٢٦ نانومتر. وأشارت القياسات البصرية إلى أن الامتصاص ومعامل الامتصاص زادا مع زيادة عدد الرشات،

JOBS مجلة العلوم الأساسية
Journal of Basic Science
Print -ISSN 2306-5249
Online-ISSN 2791-3279
العدد السادس والأربعون
٢٠٢٦م /١٤٤٨هـ

بينما انخفضت النفاذية من حوالي ٦٠% إلى ٤٣%. وانخفضت فجوة النطاق البصري من ٣,١٠ إلكترون فولت للعينة S1 إلى ٢,٩٣ إلكترون فولت للعينة S3، مصحوبة بزيادة في معامل الخمود. تُظهر النتائج أن التحكم في عدد الرشات يوفر طريقة فعالة لتعديل الأداء التركيبي والبصري لأغشية أكسيد الزنك الرقيقة. وقد أظهر غشاء S3 أفضل الخصائص العامة، مما يجعله مرشحاً واعداً لتطبيقات الإلكترونيات الضوئية وأجهزة الكشف الضوئي.

الكلمات المفتاحية: أغشية أكسيد الزنك الرقيقة، الرش الحراري الكيميائي، حيود الأشعة السينية، المجهر الإلكتروني الماسح ذو الانبعاث الميداني، مجهر القوة الذرية، الخصائص البصرية، طاقة فجوة النطاق.

Impact of Spray Cycles on Crystallinity, Structural Defects, and Optical Performance of ZnO Thin Films Deposited by Chemical Spray Pyrolysis

Asst. Lect. Ahmed turki abdulhameed[1], Lect. Dr. Muatazbullah Ibrahim Abdullah[2], Lect. Dr. Shahed A. Dheyab[3]
[1]Department of physics, college of Education for Pure Science, University of Al-Hamdaniya, Mosul, Iraq, [2]Ministry of Education Directorate General of Education in Kirkuk, Al-Jawhara Intermediate School for Girls, Kirkuk, Iraq, [3]Department of Physics, College of Education for Pure Sciences, Tikrit University, Tikrit, Iraq
Phy.ahmedturki@uohamdaniya.edu.iq[1], mutazalalmi1990@gmail.com[2], shahed.ahmed@tu.edu.iq[3]

Abstract:

ZnO thin films were deposited on glass substrates by chemical spray pyrolysis using number of spray cycles (20, 25, and 30), designated as S1, S2, and S3, respectively. The influence of the number of spray cycles on the structural, morphological, and optical properties of the films was investigated using X-ray diffraction (XRD), field emission scanning electron microscopy (FESEM), atomic force microscopy (AFM), and UV-Vis spectroscopy. XRD analysis confirmed the formation of single phase polycrystalline ZnO with a hexagonal wurtzite structure. Increasing the number of spray cycles enhanced the crystallinity, resulting in an increase in crystallite size from 27.7 to 34.1 nm, while the microstrain and dislocation density decreased from 4.45 × 10^{-3} to 3.48 × 10^{-3} and from 1.31 × 10^{15} to 0.86 × 10^{15} m^{-2}, respectively. FESEM observations revealed grain growth from approximately 160 nm to 350 nm with improved film compactness and surface homogeneity. AFM results showed an increase in the maximum surface height from 61.57 to 84.26 nm. Optical measurements indicated that absorbance and absorption coefficient increased with increasing number of spray cycles, whereas transmittance decreased from about 60% to 43%. The optical band gap decreased from 3.10 eV for S1 to 2.93 eV for S3, accompanied by an increase in the extinction coefficient. The results demonstrate that controlling the number of spray cycles provides an effective route for tailoring the structural and optical performance of ZnO thin films. The S3 film exhibited the best overall characteristics, making it a promising candidate for optoelectronic and photodetector applications.

Keywords: ZnO thin films, Chemical spray pyrolysis, XRD, FESEM, AFM, Optical properties, Band gap energy.

1. Introduction

Zinc oxide (ZnO) has emerged as one of the most extensively investigated semiconductor materials owing to its unique combination of optical transparency, chemical stability, environmental compatibility, and wide direct band gap of approximately 3.37 eV at room temperature. In addition, its large exciton binding energy (~60 meV) enables efficient excitonic emission even at ambient conditions, making ZnO a highly attractive material for advanced optoelectronic applications, including ultraviolet photodetectors, transparent electronics, solar cells, light-emitting devices, gas sensors, and photocatalytic systems (Mohammed, Abdullah, Kamil, Hussain, & Kareem, 2025), (Alasmari, Abanob, & Aboud, 2024), (Victor, et al., 2022).

The remarkable performance of ZnO based devices is strongly dependent on the structural quality, surface morphology, grain size, and defect concentration of the deposited films. Variations in these parameters can significantly influence charge transport, optical absorption, carrier recombination, and overall device efficiency. Consequently, considerable research efforts have been devoted to tailoring the microstructure and optical response of ZnO thin films through precise control of deposition conditions and post treatment processes. (Aboud, Al-Dossari, AbdEL-Gawaad, & Magdi, 2023), (Shahriari & Raeisi, 2025).

Among the various deposition techniques available for ZnO fabrication, including pulsed laser deposition, magnetron sputtering, molecular beam epitaxy, and sol-gel processing, chemical spray pyrolysis (CSP) has attracted particular attention because of its simplicity, low production cost, scalability, and suitability for large area deposition. Furthermore, CSP allows excellent control over film thickness and microstructural evolution through adjustment of deposition parameters such as substrate temperature, precursor concentration, spray rate, nozzle to substrate distance, and deposition cycles. (Sriram, Parne, Pothukanuri, & Edla, 2022), (Ravikumar & Sivaperuman, 2024), (Dimitriou, Psathas, Solakidou, & Deligiannakis, 2023).

Previous studies have demonstrated that film thickness plays a crucial role in determining the crystallinity, grain growth behavior, and optical characteristics of ZnO thin films. However, despite extensive investigations on spray deposited ZnO, the specific influence of spray number on the simultaneous evolution of crystallite size, lattice strain, dislocation density, grain morphology, and optical constants remains insufficiently understood. Establishing such correlations is essential for optimizing ZnO films intended for optoelectronic and photonic applications. (Toma, Rahman, & Maria, 2025), (Bakry, Ismail, Abdelfatah, & El-Shaer, 2024).

In the present work, ZnO thin films were deposited onto glass substrates by chemical spray pyrolysis using numbers of spray cycles (20, 25, and 30). The influence of the number of spray cycles on the structural, morphological, and optical properties of the deposited films was systematically investigated using X-ray diffraction (XRD), field emission scanning electron microscopy (FESEM), atomic force microscopy (AFM), and UV-Vis spectroscopy. Particular attention was devoted to elucidating the relationship between film growth, defect reduction, grain development, and optical performance in order to identify the deposition conditions that yield ZnO thin films with superior characteristics.

2. Experimental Procedure

2.1 Preparation of ZnO Thin Films

Zinc oxide (ZnO) thin films were deposited onto glass substrates using the Chemical Spray Pyrolysis (CSP) technique. A 0.1 Molar ratio precursor solution was prepared by dissolving 2.703 g of zinc acetate dihydrate (Zn $(CH_3COO)_2.2H_2O$, purity ≥99%) in 250 mL of distilled water under continuous magnetic stirring for 10 min at room temperature until a homogeneous solution was obtained.

2.2 Substrate Cleaning

Glass slides were cut into dimensions of 2.5 × 2.5 cm^2 and cleaned sequentially using detergent solution, distilled water, and acetone in an ultrasonic bath for 10 min each. The substrates were then dried in air prior to deposition.

2.3 Thin Film Deposition

The cleaned substrates were placed on a temperature-controlled hot plate maintained at 400 ± 2 °C. The precursor solution was sprayed using an air-brush atomizer positioned 30 cm above the substrate surface. Compressed air at a pressure of 1.5-2 bar was used as the carrier gas. The spray process consisted of 20 s spray intervals followed by 120 s pauses to maintain substrate temperature and ensure complete thermal decomposition of the precursor droplets. The spray rate was approximately 6 mL min^{-1}. Different film thicknesses were obtained by varying the number of spray cycles (20, 25, and 30). After deposition, the samples were allowed to cool naturally on

JOBS
مجلة العلوم الأساسية
Journal of Basic Science
Print -ISSN 2306-5249
Online-ISSN 2791-3279
العدد السادس والأربعون
٢٠٢٦م /١٤٤٨هـ

the heater surface to room temperature. As shown in Table 1, the ZnO thin films were categorized into three according to the number of sprays: S1 (20 spray), S2 (25 spray), and S3 (30 spray)

Table 1. Sample designation and corresponding number of spray cycles.

number of spray cycles	Sample Code
20	S1
25	S2
30	S3

2.4 Thickness Measurement

The film thickness was estimated using the gravimetric method according to:

$$t = \frac{(W_2 - W_1)}{\rho A}$$

where t is the film thickness, W_1 and W_2 are the substrate weights before and after deposition, respectively, ρ is the material density, and A is the coated area.

Table 2. Thickness of ZnO thin films deposited using different numbers of sprays

Sample	Number of sprays	Film thickness, mean ± SE (nm)	Error (%)
S1	20	250 ± 0.95	0.38
S2	25	300 ± 1.22	0.41
S3	30	350 ± 1.64	0.47

2.5 Structural Characterization

The crystal structure of the deposited ZnO films was investigated using X-ray diffraction (XRD) with Cu-Kα radiation (λ = 1.5406 Å). The crystallite size (D) was estimated using the Debye-Scherrer equation: $D = \frac{0.9\lambda}{\beta cos\theta}$, where D is the crystallite size (nm), λ is the X-ray wavelength (1.5406 Å for Cu-Kα radiation), β is the full width at half maximum (FWHM) expressed in radians, and θ is the Bragg diffraction angle. The microstrain (ε) was calculated from: $\varepsilon = \frac{\beta}{4tan\theta}$, where ε is the microstrain, β is the FWHM (radians), and θ is the Bragg angle. while the dislocation density (δ) was determined using: $\delta = \frac{1}{D^2}$, where δ is the dislocation density (lines m^{-2}) and D is the crystallite size.

2.6 Morphological Characterization

The surface morphology and grain distribution of the films were examined using Field Emission Scanning Electron Microscopy (FESEM). Surface topography, grain size distribution, and roughness parameters were analyzed using Atomic Force Microscopy (AFM).

2.7 Optical Characterization

The optical properties were investigated using a UV-Vis spectrophotometer in the wavelength range of 300-1100 nm. The absorbance (A) and transmittance (T) spectra were recorded. The absorption coefficient (α) was calculated from: $\alpha = \frac{2.303A}{t}$, where α is the absorption coefficient (cm^{-1}), A is the absorbance, and t is the film thickness (cm). The optical band gap energy (Eg) was estimated using the Tauc relation: $(\alpha hv)^2 = B(hv - Eg)$, where α

JOBS
مجلة العلوم الأساسية
Journal of Basic Science
Print -ISSN 2306-5249
Online-ISSN 2791-3279
العدد السادس والأربعون
٢٠٢٦م /١٤٤٨هـ

is the absorption coefficient, hν is the photon energy (eV), B is a material-dependent constant, and Eg is the optical band gap energy (eV). The extinction coefficient (k) was determined from: $k = \frac{\alpha\lambda}{4\pi}$, where k is the extinction coefficient, α is the absorption coefficient (cm^{-1}), and λ is the wavelength of the incident radiation (nm). Figure 1. shows the complete work flow of ZnO thin film preparation and characterization adopted in the present investigation.

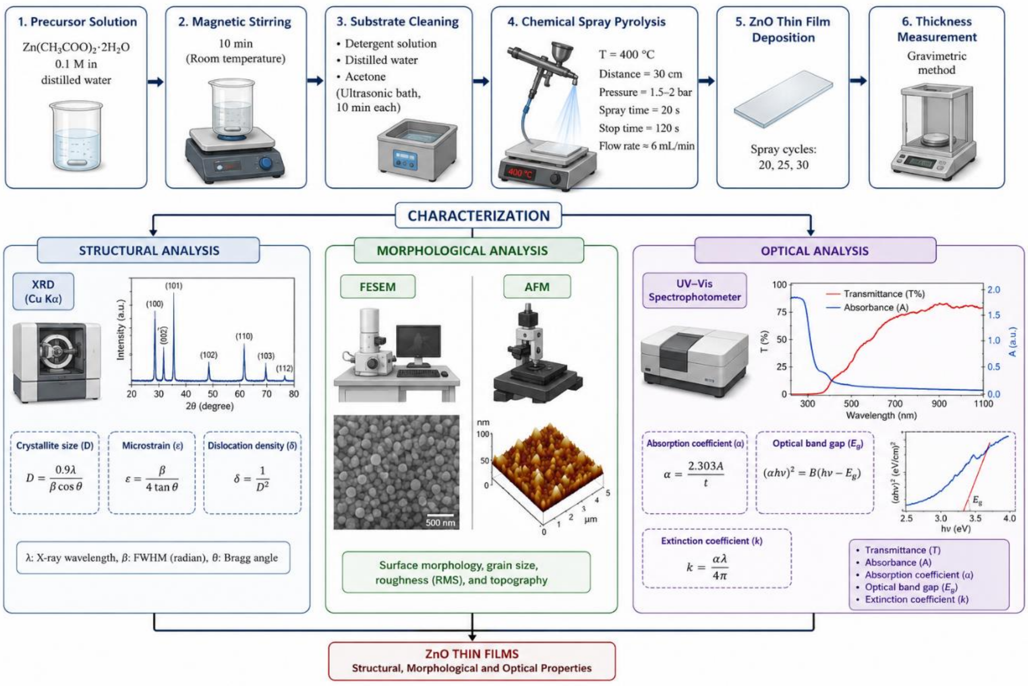

Figure 1. Schematic of ZnO thin film fabrication by chemical spray pyrolysis and subsequent structural, morphological, and optical characterization procedures.

3. Results and Discussion

3.1 X-ray diffraction Results

Figure 2 shows the X-ray diffraction (XRD) patterns of ZnO thin films deposited with numbers of spray cycles, namely S1 (20 sprays), S2 (25 sprays), and S3 (30 sprays). All diffraction peaks can be indexed to the hexagonal wurtzite structure of ZnO, confirming the successful formation of polycrystalline ZnO films without the appearance of secondary phases or impurity-related peaks. The major diffraction peaks observed at approximately 2θ = 31.8°, 34.4°, and 36.3° correspond to the (100), (002), and (101) crystallographic planes, respectively, in good agreement with the standard diffraction data reported in JCPDS Card No. 36-1451. These are characteristic reflections of hexagonal ZnO. (Hussain & Abdullah, 2023). As shown in Figure 2, the diffraction peak intensity increases progressively from S1 to S3, indicating an improvement in crystallinity with increasing number of spray cycles. This behavior can be attributed to the increase in deposited material and film thickness, which promotes crystal growth and facilitates atomic diffusion during film formation. (Cuadra, et al., 2023). Furthermore, the narrowing of diffraction peaks with increasing number of spray cycles suggests the growth of larger crystallites and a reduction in lattice imperfections. The calculated crystallite size (D), average microstrain (ε), and dislocation density (δ) are presented in Figure 3. The average crystallite size increased from approximately 27.7 nm for S1 to 30.5 nm for S2 and reached 34.1 nm for S3. The enlargement of crystallite size indicates enhanced grain growth and improved crystal ordering as the number of spray cycles increased. In contrast, the average microstrain decreased from 4.45×10^{-3} for S1 to 3.95×10^{-3} for S2 and further to 3.48×10^{-3} for S3. The reduction in microstrain suggests a gradual relaxation of lattice distortion and a decrease in internal stresses within the ZnO lattice. (Rincon-Suarez, et al., 2025). The dislocation density decreased from approximately 1.31×10^{15} m^{-2} for S1 to 1.08×10^{15} m^{-2} for S2 and 0.86×10^{15} m^{-2} for S3. Since dislocation density is inversely proportional to the square of crystallite size, the observed reduction confirms the enhancement of crystal quality and the

JOBS
مجلة العلوم الأساسية
Journal of Basic Science
Print -ISSN 2306-5249
Online-ISSN 2791-3279
العدد السادس والأربعون
٢٠٢٦م /١٤٤٨هـ

reduction of structural defects with increasing film thickness. (Mahajan & Gumfekar, 2026).

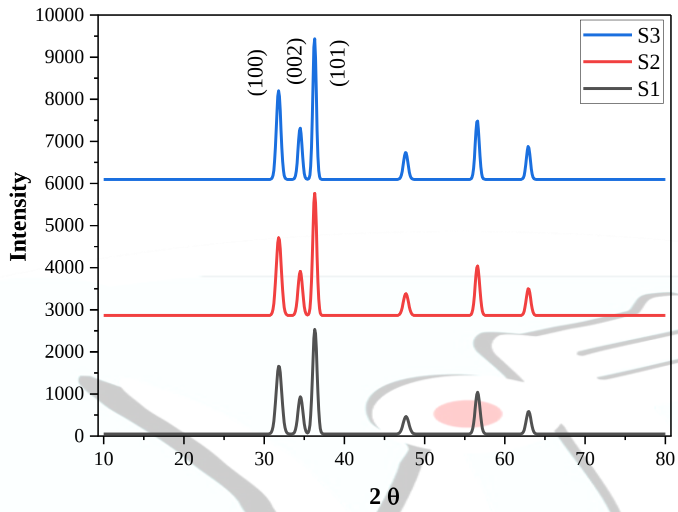

Figure 2. XRD patterns of ZnO thin films deposited with number of spray cycles (S1, S2, and S3).

JOBS
مجلة العلوم الأساسية
Journal of Basic Science
Print -ISSN 2306-5249
Online-ISSN 2791-3279
العدد السادس والأربعون
٢٠٢٦م /١٤٤٨هـ

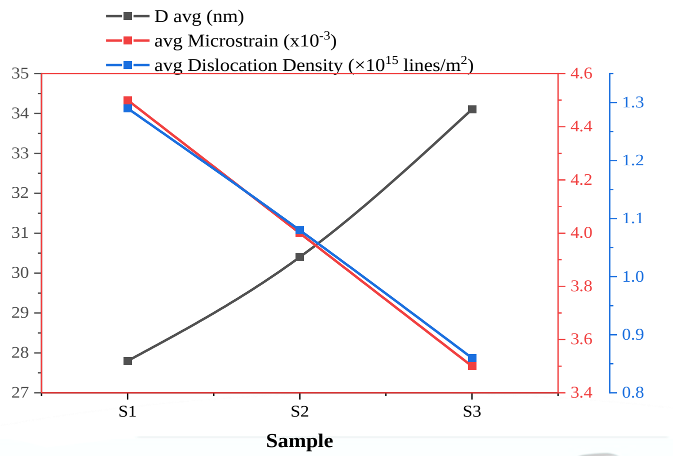

Figure 3. Variation of average crystallite size, microstrain, and dislocation density of ZnO thin films as a function number of spray cycles.

3.2 Field Emission Scanning Electron Microscope (FESEM)

Figure 4 shows the FESEM micrographs of ZnO thin films prepared with a number of spray cycles, namely S1 (20 spray), S2 (25 spray), and S3 (30 spray). It is evident from Figure 4 that the surface morphology of the deposited films is strongly influenced by the number of spray cycles, which affects the film thickness, grain growth, and surface compactness. The S1 film exhibits a relatively heterogeneous surface consisting of irregularly shaped grains with an average grain size of approximately 160 nm to 350 nm. The grains are distributed non uniformly, and noticeable voids can be observed between neighboring grains, indicating incomplete grain coalescence during the early stages of film growth. Such morphology is characteristic of relatively thin films deposited with a limited amount of precursor material. When the number of spray cycles was increased to 25 (S2), the morphology changed considerably, as shown in Figure 4(b). The surface became more compact and homogeneous, while the grains became more spherical and had a narrower size distribution. The average grain size increased to approximately 300 nm, indicating enhanced grain growth and improved crystal development. The reduction in intergranular voids suggests

JOBS مجلة العلوم الأساسية
Journal of Basic Science
Print -ISSN 2306-5249
Online-ISSN 2791-3279
العدد السادس والأربعون
٢٠٢٦م /١٤٤٨هـ

that the additional deposited material promoted grain coalescence and improved surface coverage. (Fayaz Rouhi & Rozati, 2022). Further increasing the number of spray cycles to 30 (S3) produced a pronounced change in film morphology, as shown in Figure 4(c). The film surface shows densely packed grains with well-defined grain boundaries and an average grain size of approximately 350 nm. The larger grain size reflects continued grain growth due to increased film thickness and prolonged deposition. The film exhibits a highly compact structure with minimal porosity, indicating improved crystallinity and structural stability. (Chandak, Kumbhar, Talekar, Gunjakar, & Kulal, 2024). The progressive increase in grain size agrees well with the XRD results in Figure 3, where crystallite size increased while microstrain and dislocation density decreased with increasing spray-cycle number. This behavior suggests that the larger amount of deposited material facilitates atomic diffusion and grain-boundary migration, improving crystal quality and reducing structural defects.

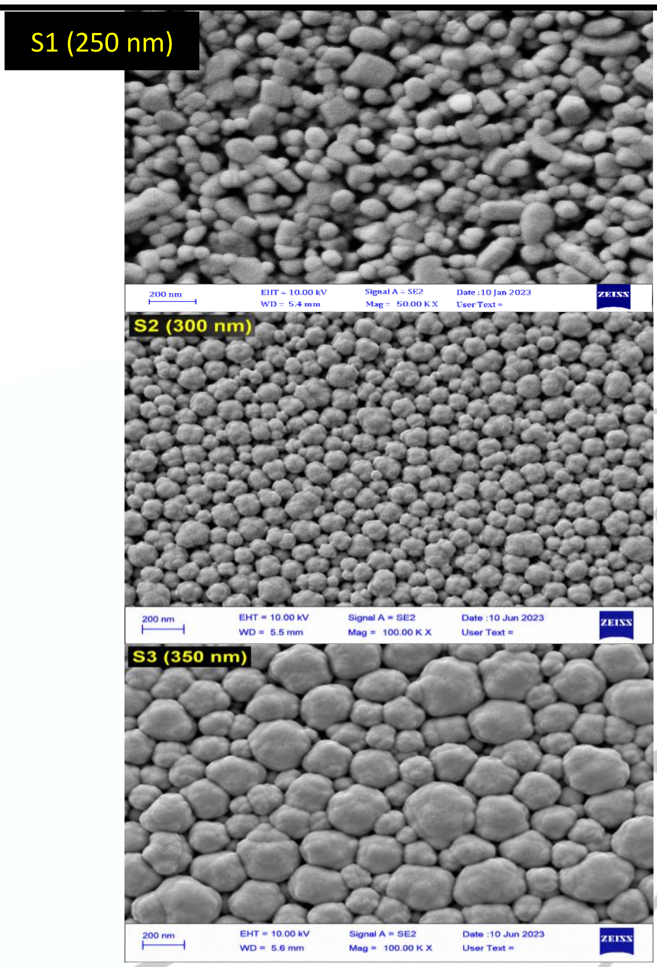

Figure 4. FESEM images of ZnO thin films prepared with number of spray cycles.

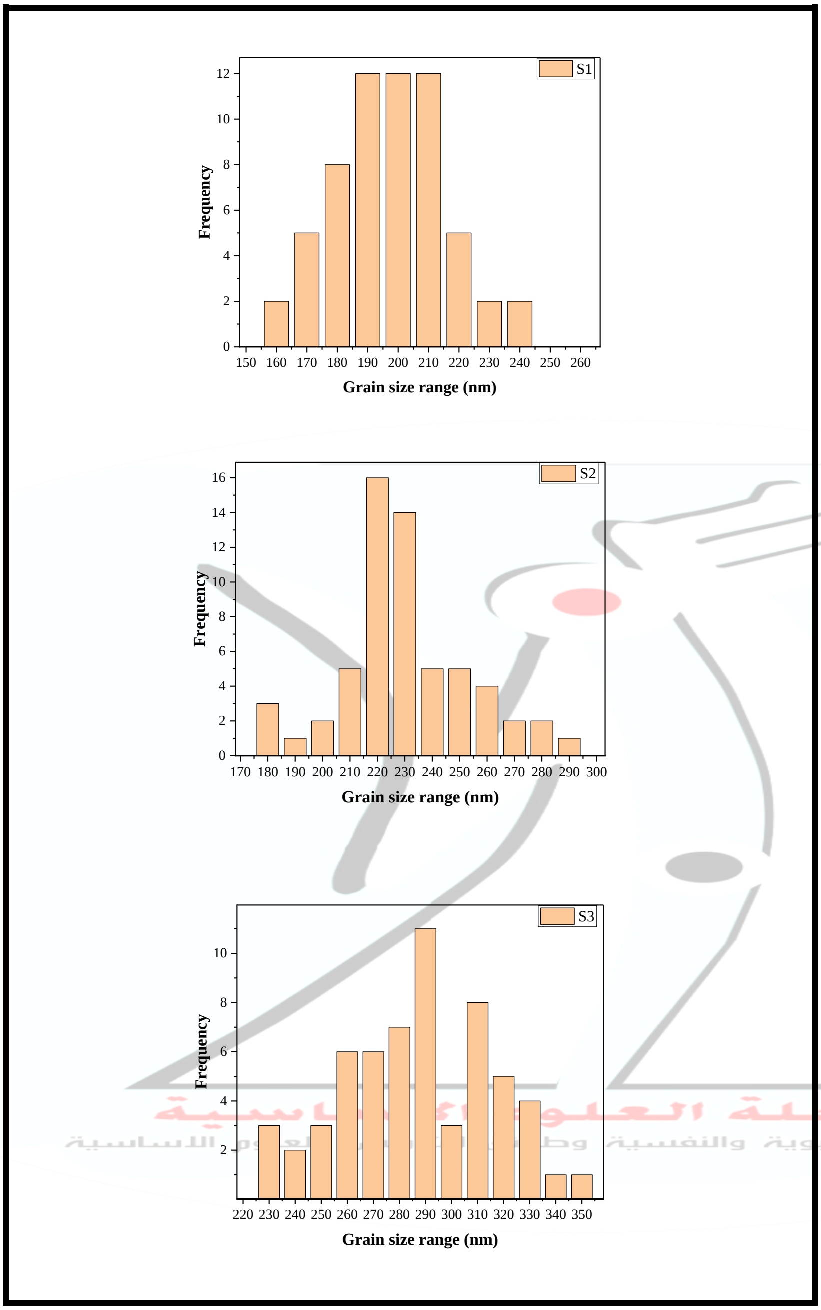
S1
Frequency
Grain size range (nm)
S2
Frequency
Grain size range (nm)
S3
Frequency
Grain size range (nm)

3.3 Atomic Force Microscopy (AFM) Results

The surface topography and grain growth behavior of the ZnO thin films were further investigated using Atomic Force Microscopy (AFM). The AFM images of samples S1, S2, and S3 are presented in Figure 5. The obtained images reveal significant changes in surface morphology with increasing number of spray cycles, confirming the influence of film thickness on the microstructural evolution of the deposited ZnO films. The S1 film exhibits a relatively fine granular structure with uniformly distributed nanosized grains over the entire scanned area. The maximum surface height recorded for this sample was approximately 61.57 nm. The relatively small grain dimensions indicate that grain nucleation dominates over grain growth during the early stages of film formation. For sample S2, the grains become noticeably larger and more densely packed compared with S1. The surface appears more homogeneous and compact, while the maximum surface height increases to approximately 72.83 nm. This behavior suggests that increasing the number of spray cycles provides additional deposited material that promotes grain coalescence and lateral grain growth. (Rabeel et al., 2022). A further increase in the number of spray cycles to 30 (sample S3) produces substantial grain enlargement. The surface is characterized by larger, hill-like grains distributed uniformly across the substrate. The maximum surface height reaches approximately 84.26 nm, indicating a significant increase in grain growth and surface development. The formation of larger grains is attributed to enhanced atomic diffusion and grain boundary migration during successive deposition cycles. (Bouras, Beggas, Sahnoune, Ghougali, & Ferhat, 2024). The AFM observations are consistent with the FESEM and XRD results discussed previously. The increase in grain dimensions from S1 to S3 corresponds to the increase in crystallite size and the reduction in microstrain and dislocation density obtained from XRD analysis. The larger grains in S3 indicate improved crystallinity and a reduced defect concentration within the ZnO lattice.

JOBS مجلة العلوم الأساسية
Journal of Basic Science
Print -ISSN 2306-5249
Online-ISSN 2791-3279
العدد السادس والأربعون
٢٠٢٦م /١٤٤٨هـ

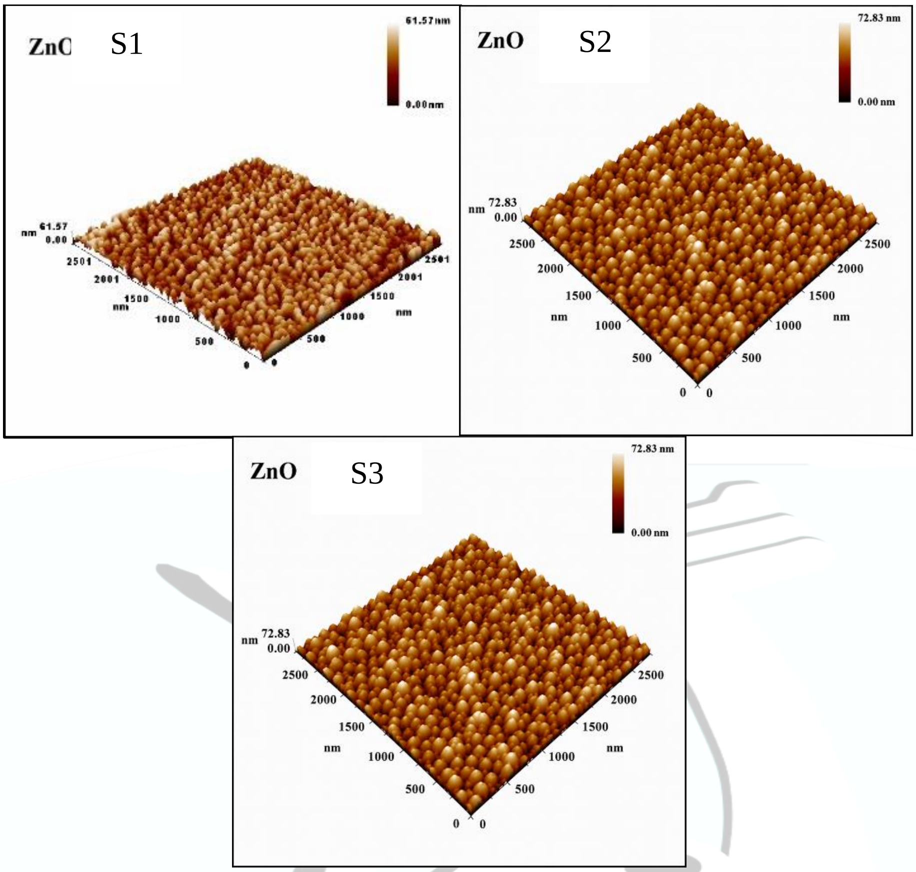

Figure 5. AFM images of ZnO thin films deposited with number of spray cycles.

3.4 Optical Properties

3.4.1 Absorbance Spectra

The optical absorbance spectra of ZnO thin films deposited with many spray cycles are shown in Figure 6. All samples exhibit relatively high absorbance in the short-wavelength region, followed by a gradual decrease with increasing wavelength. This behavior is characteristic of ZnO semiconductor films and is associated with the fundamental electronic transitions occurring near the absorption edge. (Nikam, et al., 2022). The absorbance increases systematically with increasing number of spray cycles. Sample S3 exhibits the highest absorbance throughout the investigated spectral range, followed by S2 and S1. At a wavelength of approximately 400 nm, the absorbance values reach nearly 0.98, 0.85, and 0.75 for S3, S2, and S1, respectively. The enhanced absorbance of S3 can be attributed to the increased film thickness and improved crystallinity, as confirmed by the XRD and FESEM analyses. Thicker films provide a longer optical path for incident photons, resulting in greater light absorption within the material. (Hambi, et al., 2024). The gradual increase in absorbance with the number of spray cycles suggests a higher density of absorbing centers and a reduction in light scattering losses due to the improved compactness and uniformity of the film surface.

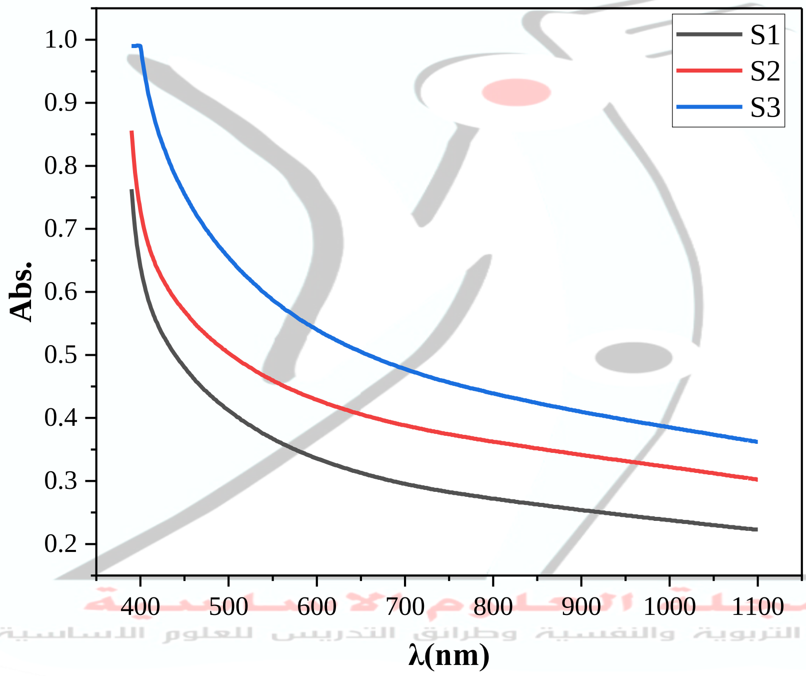

Figure 6. Absorbance spectra of ZnO thin films deposited with number of spray cycles.

3.4.2 Transmittance Spectra

Figure 7 shows the optical transmittance spectra influence of the number of spray cycles of the ZnO thin films in the wavelength range of 400-1100 nm. The transmittance of all samples increases gradually with increasing wavelength, indicating reduced photon absorption in the low-energy region of the spectrum. Sample S1 exhibits the highest transmittance values over the entire investigated wavelength range, reaching approximately 60% at 1100 nm. Samples S2 and S3 display lower transmittance values of approximately 50% and 43%, respectively. The decrease in transmittance with increasing spray cycles is mainly attributed to the increase in film thickness and grain size, which enhance photon absorption and reduce the amount of transmitted light. (Allag, et al., 2024). The inverse relationship observed between absorbance and transmittance is consistent with Beer-Lambert theory, where an increase in absorbed optical energy results in a corresponding decrease in transmitted radiation. The lower transmittance of S3 is therefore a direct consequence of its higher absorbance and larger grain size. (Aboud A. A., Al-Dossari, AbdEL-Gawaad, & Magdi, 2023). The optical measurements indicate that increasing the number of spray cycles enhances the light-harvesting capability of ZnO thin films by increasing absorbance and reducing transmittance. These characteristics are favorable for optoelectronic and photodetection applications requiring efficient photon absorption.

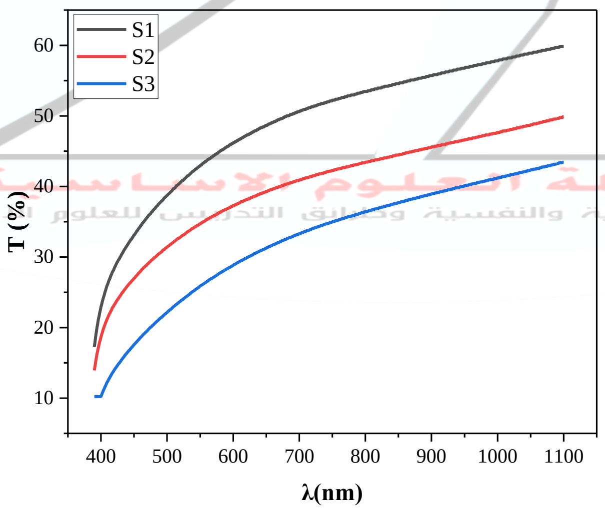

Figure 7. Transmittance spectra of ZnO thin films deposited with several spray cycles.

JOBS مجلة العلوم الأساسية
Journal of Basic Science
Print -ISSN 2306-5249
Online-ISSN 2791-3279
العدد السادس والأربعون
٢٠٢٦م /١٤٤٨هـ

3.4.3 Absorption Coefficient Analysis

The variation of the absorption coefficient (α) as a function of photon energy for ZnO thin films deposited with several spray cycles is shown in Figure 8. The absorption coefficient increases gradually with increasing photon energy for all samples, reaching its maximum value near the fundamental absorption edge of ZnO. This behavior is attributed to the increased probability of electronic transitions from the valence band to the conduction band as the incident photon energy approaches the band gap energy. The absorption coefficient values of samples S2 and S3 are consistently higher than those of S1 throughout the investigated energy range. This increase can be attributed to the greater film thickness, improved crystallinity, and enhanced grain growth observed in the structural and morphological analyses. The larger grains and denser microstructure facilitate stronger photon interaction within the films, thereby increasing optical absorption. (Alsaiari, Awad, Ismail, & Aboud, 2024). At higher photon energies, a sharp increase in α is observed for all samples, indicating the onset of direct allowed electronic transitions characteristic of ZnO semiconductors. The obtained absorption coefficient values 10^4 cm^{-1}, confirming the strong optical absorption behavior of the deposited films and their suitability for optoelectronic applications. (Salim & Azzaoui, 2023).

JOBS
مجلة العلوم الأساسية
Journal of Basic Science
Print -ISSN 2306-5249
Online-ISSN 2791-3279
العدد السادس والأربعون
٢٠٢٦م /١٤٤٨هـ

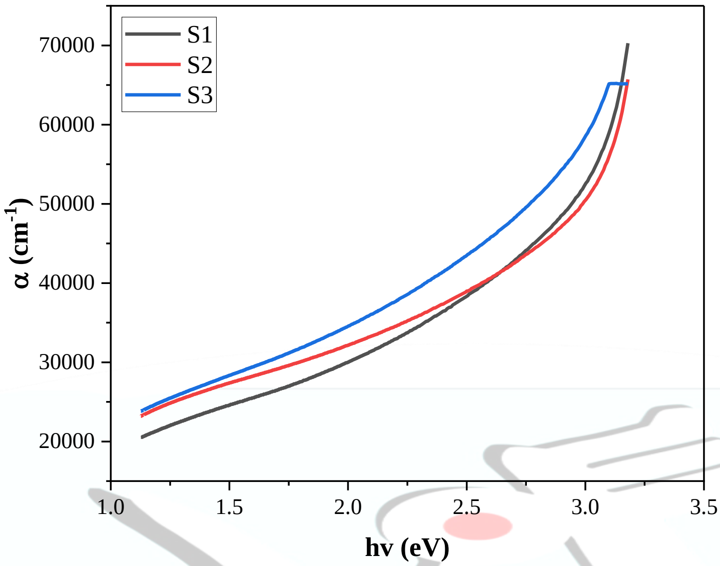

Figure 8. Absorption coefficient spectra of ZnO thin films deposited with a number of spray cycles.

3.4.4 Optical Band Gap Analysis

Figure 9 shows the optical band gap energy of the ZnO thin films. The calculated band gap values decreased progressively from approximately 3.10 eV for S1 to 3.04 eV for S2 and 2.93 eV for S3 as the number of spray cycles increased. This narrowing can be attributed to the combined effects of increasing film thickness and crystallite size on the electronic structure of the films. The growth of larger crystallites reduces the density of grain boundaries and weakens carrier confinement and grain-boundary scattering, allowing the optical behavior to approach that of a more continuous polycrystalline film. At the same time, increasing thickness modifies the distribution of structural imperfections and localized electronic states near the valence- and conduction-band edges, resulting in an extension of the band-tail states and a red shift of the absorption edge toward lower photon energies. To evaluate these localized states, the Urbach energy was determined from the linear dependence of ln(α) on photon energy. The obtained EU values were 1.098, 1.267, and 1.166 eV for S1, S2, and S3, respectively. The increase observed for S2 indicates a greater contribution from localized tail states and structural disorder, whereas the subsequent decrease for S3 suggests partial improvement in structural ordering and crystallite growth. However, the Urbach energy of S3 remained higher than that of S1, demonstrating that localized states continued to contribute to the observed red shift and band-gap narrowing. Therefore, the progressive reduction in the optical band gap cannot be attributed to a single structural parameter but results from the combined influence of film thickening, crystallite growth, reduced grain-boundary density, and the evolution of localized band-tail states. The obtained values remain within the range reported for polycrystalline ZnO thin films prepared by spray pyrolysis and related deposition techniques (Ahmed et al., 2024; Boussaada et al., 2024).

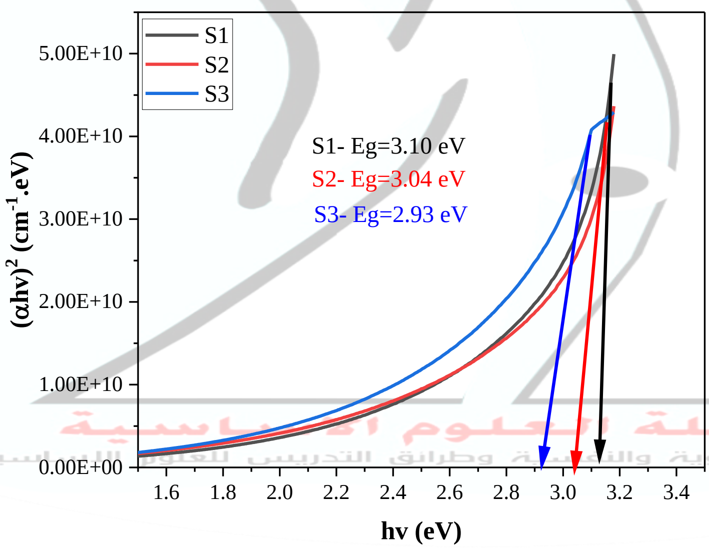

Figure 9. Optical band gap energy of the deposited ZnO films.

3.4.5 Extinction Coefficient Results

Figure 10 shows the variation of the extinction coefficient (k) as a function of wavelength for ZnO thin films prepared with a number of spray cycles. All samples exhibit relatively high (k) values in the ultraviolet region, followed by a rapid decrease in the visible range and a gradual increase

JOBS
مجلة العلوم الأساسية
Journal of Basic Science
Print -ISSN 2306-5249
Online-ISSN 2791-3279
العدد السادس والأربعون
٢٠٢٦م /١٤٤٨هـ

toward longer wavelengths. The extinction coefficient increases systematically from S1 to S3 over the entire wavelength range. Sample S3 exhibits the highest (k) values, whereas S1 shows the lowest values. This behavior is consistent with the absorbance spectra discussed previously, since the extinction coefficient is directly related to the absorption coefficient. The increase in (k) with increasing number of spray cycles is attributed to the higher film thickness, improved crystallinity, and enhanced grain growth. The larger grains observed in the FESEM and AFM analyses promote stronger interaction between incident photons and the ZnO lattice, leading to increased optical attenuation within the films. (Alattar, Abbas, & Al-Azawy, 2025). The optical analyses demonstrate that increasing the number of spray cycles enhances the absorption capability of ZnO thin films, increases the extinction coefficient, and slightly reduces the optical band gap energy. These changes indicate improved optical activity and suggest the suitability of the deposited films for photovoltaic, photodetector, and optoelectronic applications.

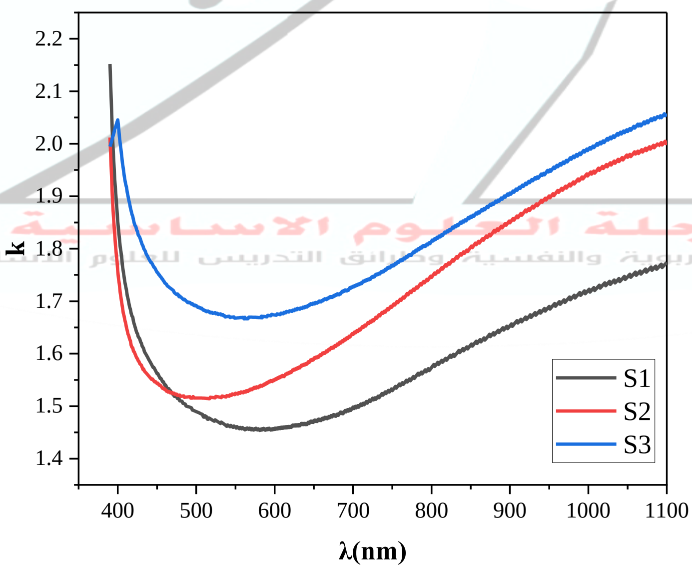

Figure 10. Variation of the extinction coefficient as a function of wavelength.

JOBS مجلة العلوم الأساسية
Journal of Basic Science
Print -ISSN 2306-5249
Online-ISSN 2791-3279
العدد السادس والأربعون
٢٠٢٦م /١٤٤٨هـ

4. Conclusions

ZnO thin films were successfully deposited on glass substrates by the chemical spray pyrolysis technique using a number of spray cycles (20, 25, and 30). XRD analysis confirmed the formation of polycrystalline ZnO films with a hexagonal wurtzite structure. Increasing the number of spray cycles improved the structural quality of the films, resulting in an increase in crystallite size from approximately 27.7 nm to 34.1 nm, accompanied by a reduction in microstrain from 4.45×10^{-3} to 3.48×10^{-3} and dislocation density from 1.31×10^{15} to 0.86×10^{15} lines m^{-2}. FESEM and AFM investigations revealed significant grain growth and surface development with increasing spray cycles. The average grain size increased from approximately 160 nm for S1 to 350 nm for S3, while the maximum surface height increased from 61.57 to 84.26 nm, indicating enhanced grain coalescence and improved film compactness. Optical measurements showed that the absorbance increased, whereas the transmittance decreased with increasing number of spray cycles, reflecting the influence of film thickness and microstructural evolution on light-matter interaction. The optical band gap decreased from 3.10 eV for S1 to 2.93 eV for S3, which is attributed to the increase in crystallite size and the reduction of structural defects. In addition, the absorption and extinction coefficients exhibited higher values for thicker films, indicating enhanced optical activity. The ZnO thin film prepared with 30 spray (S3) exhibited the best combination of structural quality, grain growth, and optical absorption characteristics, making it a promising candidate for optoelectronic and photodetector applications.

1. **References**

2. Ahmed, A. D., Ezike, S. C., Ike, E., Idu, K. H., Obodo, R. M., & Salawu, M. A. (2024, 3 1). Spray pyrolyzed surface-modified ZnO thin films via cobalt doping: Optical, structural and morphological properties. *Optical Materials*, p. 115053.

3. Alattar, A. M., Abbas, S. I., & Al-Azawy, A. A. (2025, 6 18). Nanoparticles Prepared by Spray Pyrolysis Technology for UV Detector Improvement: Study Bacterial Activity with Medical Physics. *Plasmonics*, pp. 1575–1589.

4. Allag, N., Bouafia, A., Chemsa, B., Ben Mya, O., Chala, A., Siad, C., & Alam, M. W. (2024, 10 26). Effect of precursors on structural, optical and surface properties of ZnO thin film prepared by spray pyrolysis method: efficient removal of Cu (II) from wastewater. *Transition Metal Chemistry*, pp. 39-51.
5. Alsaiari, N. A., Awad, A. A., Ismail, M. F., & Aboud, A. A. (2024, 12 27). Physical properties of La: ZnO thin films prepared at different thicknesses using spray pyrolysis technique. *Physica Scripta*, p. 1059d8.
6. Bouras, L., Beggas, A., Sahnoune, D., Ghougali, M., & Ferhat, R. (2024, 11 11). High optimization of crystallization experimental conditions of ZnO nano thin films prepared by spray pyrolysis technique for optoelectronic applications. *Chalcogenide Letters*, pp. 917 - 926.
7. Fayaz Rouhi, H., & Rozati, S. M. (2022, 3 2). Synthesis and investigating effect of tellurium-doping on physical properties of zinc oxide thin films by spray pyrolysis technique. *Applied Physics A*, p. 252.
8. Hambi, M., Khadraoui, M., Miloua, R., Bouzidi, A., Nakrela, A., Medles, M., & Amara, Z. (2024, 10 1). Structural evolution and photocatalytic performance of ZnS–ZnO thin films synthesized by spray pyrolysis. *Ceramics International*, pp. 35902-35914.
9. Mahajan, C. M., & Gumfekar, S. P. (2026, 5 1). Unveiling the evolution of microstructural and optoelectronic properties of spray-pyrolyzed ZnO thin films via tailoring the aerosol deposition time. *The Canadian Journal of Chemical Engineering*, pp. 2352-2364.

10. Mohammed, W. M., Abdullah, Q. N., Kamil, M. A., Hussain, A. A., & Kareem, M. Q. (2025, 11 1). Enhanced broadband photo-detection via carbon nanotube integration in ZnO nanostructured films. *Physica B: Condensed Matter*, p. 417655.
11. Rabeel, M., Javed, S., Khan, R., Akram, M. A., Rehman, S., Kim, D.-k., & Khan, M. F. (2022, 5 7). Controlling the Wettability of ZnO Thin Films by Spray Pyrolysis for Photocatalytic Applications. *Materials*, p. 3364.
12. Salim, K., & Azzaoui, W. (2023, 5 3). Physical properties of spray pyrolysed ZnO thin films obtained from nitrate, acetate and chloride precursors: Comparative study for Solar Cell Applications. *Revista mexicana de física*, pp. 0-0.
13. Aboud, A. A., Al-Dossari, M., AbdEL-Gawaad, N. S., & Magdi, A. (2023, 8 29). Effect of annealing on the physical properties of Co: ZnO thin films prepared by spray pyrolysis technique. *Physica Scripta*, p. 095958.
14. Alasmari, A., Abanob, A., & Aboud, A. (2024, 2 1). Investigating the influence of yttrium doping on physical properties of ZnO thin films deposited via spray pyrolysis. *Optical Materials*, p. 114899.
15. Bakry, M., Ismail, W., Abdelfatah, M., & El-Shaer, A. (2024, 10 11). Low-cost fabrication methods of ZnO nanorods and their physical and photoelectrochemical properties for optoelectronic applications. *Scientific reports*, p. 23788.
16. Boussaada, S. E., Mouchaal, Y., Riane, H., & Khelil, A. (2024, 10 1). An investigation of structural, electrical and optical properties of metal free-zinc oxide thin films using spray pyrolysis sol-gel techniques. *Egyptian Journal of Chemistry*, pp. 181-189.
17. Chandak, V. S., Kumbhar, M. B., Talekar, S. V., Gunjakar, J. L., & Kulal, P. M. (2024, 4 4). Ultrasensitive and selective Cr-doped ZnO thin films synthesized via spray pyrolysis technique for detection of ammonia gas. *Applied Physics A*, p. 285.
18. Cuadra, J. G., Estrada, A. C., Oliveira, C., Abderrahim, I. A., Porcar, S., Fraga, D., . . . Carda, J. B. (2023, 10 15). Functional properties of transparent ZnO thin films synthetized by using spray pyrolysis for environmental and biomedical applications. *Ceramics International*, pp. 32779-32788.
19. Dimitriou, C., Psathas, P., Solakidou, M., & Deligiannakis, Y. (2023, 11 23). Advanced flame spray pyrolysis (FSP) technologies for

engineering multifunctional nanostructures and nanodevices. *Nanomaterials*, p. 3006.

20. Hussain, A. A., & Abdullah, Q. N. (2023, 9 25). Studying the structural, optical and electrical properties of ZnO: SnO2 thin films as an application of a gas sensor using vacuum thermal evaporation technique. *Tikrit J. Pure Sci*, pp. 66-75.
21. Nikam, S. V., Jadhav, B. T., Chivate, S. M., Nikam, S. M., Mujawar, S. H., & Torane, A. P. (2022). Structural, morphological and optical attributes of ZnO thin films deposited via spray pyrolysis process: Impact of molarity variation. *In IOP Conference Series: Materials Science and Engineering* (p. 012012). IOP Publishing.
22. Ravikumar, T., & Sivaperuman, K. (2024, 4 5). Branched ZnFe2O4 nanorods grown via chemical spray pyrolysis technique for chemiresistive xylene gas sensor. . *Colloids and Surfaces A: Physicochemical and Engineering Aspects*, , p. 133382.
23. Rincon-Suarez, E., Mozo, J. M., Romero-López, A., Alcántara-Iniesta, S., Flores-Ruiz, F., & Serrano, L. E. (2025, 10 1). Structural, optical and electrical properties of ZnO thin films deposited in the plane direction (002) by ultrasonic spray pyrolysis using nitrogen as carrier gas. *Materials Science and Engineering: B*, p. 118430.
24. Shahriari, E., & Raeisi, M. (2025, 9 23). Structural and optical nonlinearity of ZnO: Ni thin films via chemical spray pyrolysis: Role of defects and doping concentration. *Journal of Alloys and Compounds*, p. 183513.
25. Sriram, S. R., Parne, S. R., Pothukanuri, N., & Edla, D. R. (2022, 6 1). Prospects of spray pyrolysis technique for gas sensor applications–A comprehensive review. *Journal of analytical and applied pyrolysis*, p. 105527.
26. Toma, F. Z., Rahman, M. S., & Maria, K. H. (2025, 3 15). A review of recent advances in ZnO nanostructured thin films by various deposition techniques. *Discover Materials*, p. 60.
27. Victor, A. O., Emmanuel, A., Abiodun, E. A., Ayodeji, O. S., Saheed, A. A., Adedeji, T. A., . . . Abimbola, P. I. (2022, 3 1). Effect of precursor concentration on corrosion resistance and microstructure of ZnO thin films using spray pyrolysis method. *Scientific African*, p. e01073.